

Dynamic and static structural displacement measurement using backscattering DC coupled radar

Shanyue Guan^{*1}, Jennifer A. Rice¹, Changzhi Li², Yiran Li² and Guochao Wang²

¹Engineering School of Sustainable Infrastructure and Environment, University of Florida,
Gainesville, FL, USA 32611

²Department of Electrical and Computer Engineering, Texas Tech University,
Lubbock, Texas, USA 79409

(Received September 10, 2014, Revised December 6, 2014, Accepted January 7, 2015)

Abstract. Vibration-based monitoring is one approach used to perform structural condition assessment. By measuring structural response, such as displacement, dynamic characteristics of a structure may be estimated. Often, the primary dynamic responses in civil structures are below 5 Hz, making accurate low frequency measurement critical for successful dynamic characterization. In addition, static deflection measurements are useful for structural capacity and load rating assessments. This paper presents a DC coupled continuous wave radar to accurately detect both dynamic and static displacement. This low-cost radar sensor provides displacement measurements within a compact, wireless unit appropriate for a range of structural monitoring applications. The hardware components and operating mechanism of the radar are introduced and a series of laboratory experiments are presented to assess the performance characteristics of the radar. The laboratory and field experiments investigate the effect of factors such as target distance, motion amplitude, and motion frequency on the radar's measurement accuracy. The results demonstrate that the radar is capable of both static and dynamic displacement measurements with sub-millimeter accuracy, making it a promising technology for structural health monitoring.

Keywords: DC coupled radar; dynamic displacement; static deflection; moving load test

1. Introduction

Vibration-based monitoring is a commonly proposed approach for structural condition assessment. By measuring and analyzing the responses of a structure, such as displacement, acceleration, or velocity, its dynamic characteristics may be determined. In particular, dynamic displacement measurements may be used to analyze structural dynamic characteristics, while static deflection measurements may be used for a range of applications including bridge load rating and structural stiffness estimation (Chan *et al.* 2009).

Although there are various types of sensors to measure dynamic and static displacement, existing technologies have limitations when considering accuracy and cost. For example, low-cost MEMS accelerometers are capable of measuring acceleration accurately, but result in poor displacement measurement accuracy due to errors introduced by signal integration (Stiros 2008

*Corresponding author, Ph.D. Candidate, E-mail: mmkwan@ufl.edu

and Yang *et al.* 2006). Laser Doppler Vibrometer has been used to measure bridge vibrations with high accuracy (Rossi *et al.* 2002); however, its high cost limits its wide application. Global Positioning System (GPS) and Robotic Total Station (RTS) have also been applied to monitor structural motion (Stiros and Psimoulis 2012, Moschas and Stiros 2014), but their low sampling rate may not be adequate to capture all dynamic characteristics of interest. Researchers have used high speed camera or video to measure the displacement of structures through analysis of the continuous time history photo frames. However, on cloudy days or at nighttime, the image quality is poor and makes analysis difficult (Lee and Shinozuka 2006). Detecting structural displacement with high accuracy at a low cost has proven to be challenging.

In this paper a DC coupled continuous wave (CW) radar is introduced that demonstrates promising performance for detecting both dynamic and static displacement. The DC coupled CW radar is capable of measuring displacement accurately at a relatively low cost (~300 USD per wireless sensor unit including the XBee radio), and its compact size makes installation convenient. This paper first provides the background of the DC coupled CW radar. Low frequency dynamic displacement measurement performance is characterized by laboratory experiments and the capabilities of detecting static deflections are demonstrated and characterized in both laboratory and field experiments. This paper focuses on the DC coupled CW radar, which adds low frequency displacement measurement capabilities (DC to 2 Hz) not previously realized in earlier hardware revisions. In addition, a moving load experiment is conducted to demonstrate the radar's potential for bridge monitoring applications.

2. Background

Continuous wave (CW) radar transmits a continuous microwave at a constant carrier frequency. The transmitted signal is reflected by a target, with the relative distance change between the target and the radar modulated into the radar's received signal. After processing the received signal, a time history of the relative displacement between the target and the radar can be obtained. In previous studies, an AC coupled CW radar was investigated for measuring structural displacement (Rice *et al.* 2012) after its success in medical applications, including vital sign detection (Gu *et al.* 2010) and tumor detection (Gu *et al.* 2011). However, the AC coupled radar utilizes a high pass filter that limits the detection of very low frequency (< 1.75 Hz) and static displacement. The DC coupled radar presented in this paper overcomes this challenge and as a result, this paper focuses on the very low frequency performance of the radar.

2.1 DC coupled radar hardware

The DC coupled radar consists of three major components: (1) a pair of patch antennae, (2) a radio frequency (RF) board and, (3) a baseband board. The assembled components of the radar are shown in Fig. 1. Each antenna consists of a metallic patch mounted on a larger rectangular substrate shown in Fig. 2. The dimensions of the patch are a function of the operating frequency and the properties of the substrate. For the same substrate, a lower transmission frequency results in a larger antenna size. Balancing cost and the antennae size, a 2.4 GHz carrier frequency utilizing a FR4 laminate substrate is selected to maintain a relatively small size (6.5 mm × 5.2 mm) and low cost (~100 USD per pair). Maximum RF radiation occurs normal to the patch surface while backward radiation is limited by the ground plane of the antenna. The larger the ground plane is

relative to the patch, the more gain and directivity is achieved by the antenna. The half power beam width of the antenna is conservatively estimated at 45° .

The 2.4 GHz continuous microwave is generated by a voltage-controlled oscillator (VCO) on the RF board, and transmitted by one of the patch antennae. The signal is reflected from the target and captured by the other antenna. The transmitted and received signals are combined by a mixer and the resulting signal is transferred to the baseband board. The microcontroller on the baseband board controls all system operations. The mixed signals are down converted to their baseband (I/Q) signals on the baseband board. To enable wireless communication of the measured baseband signals from the radar sensor to a central data collection PC, a pair of XBee radio modules is used. One XBee module is integrated with the baseband board of the radar and the other module is connected to a PC via USB. XBee radio modules are based on the 802.15.4 communication protocol. They may be applied for point-to-point and star communications between different nodes, providing the possibility to establish a wireless network employing up to 16 radars with current 9600 bps baud rate of the XBee module. The average price of an XBee module is ~30 USD. Depending on the specific XBee module and accompanying antennae that are used, transmission distances range from 20 m to 50 m. For 2.4 GHz DC coupled radar, a 900 MHz XBee module is used to avoid interference between the 2.4 GHz microwave generated by the radar.

The data collection at the PC is controlled by a National Instruments LabView software application. All test parameters (such as the sampling rate) are set in LabView, which enables the initiation, visualization, storage, and termination of data collection.

The required power supply voltage range for the radar is between 4.8V and 5.5V, which may be provided by a DC power supply or batteries. Four AAA batteries assembled in the battery board typically supply the power for wireless operation. Based on experimental results, using four 900 mAh AAA batteries, the radar can operate continuously for more than an hour; much longer battery operation is expected if intermittent operation and sleep cycling are employed which has been verified by Imote2 (Rice *et al.* 2010).

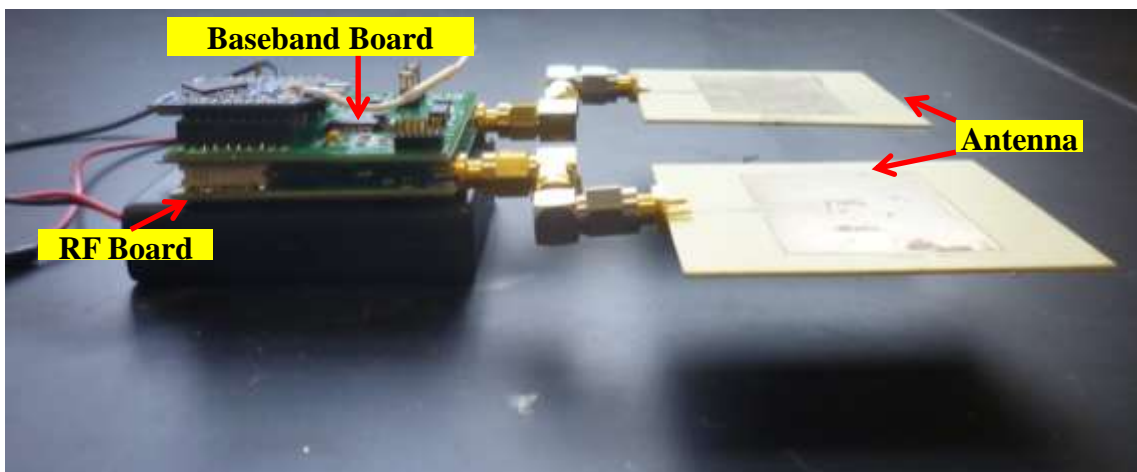


Fig. 1 Assembled components of DC Coupled radar

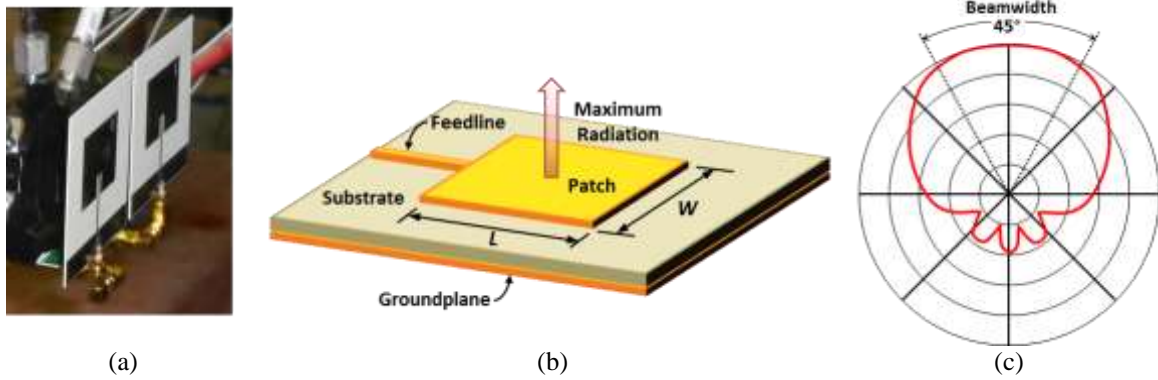


Fig. 2 (a) Picture of radar antennae, (b) antennae components and (c) estimated radiation pattern

2.2 Baseband signals

The baseband (I/Q) signals generated by the radar are given by

$$B_I(t) = A_I \cos[\theta + 4\pi x(t)/\lambda + \Delta\varphi] + DC_I \quad (1)$$

$$B_Q(t) = A_Q \sin[\theta + 4\pi x(t)/\lambda + \Delta\varphi] + DC_Q \quad (2)$$

where A_I and A_Q are the amplitudes of I and Q signals, θ is a constant phase shift due to the transmission path and target surface, $\Delta\varphi$ is the total residual phase noise of the radar, and DC_I and DC_Q are the DC offsets in I and Q baseband signals, respectively. The $4\pi x(t)/\lambda$ term is the phase information corresponding to the target movement, $x(t)$, and λ is the carrier wavelength.

2.3 DC tuning process

One of the challenges associated with the operation of the DC coupled radar is retaining the DC component of baseband signals without saturation (i.e., exceeding the limits of the analog-to-digital converter (ADC) of the microcontroller). Without proper signal adjustment prior to measurements, the magnitude of the DC component of the signal can be orders of magnitude larger than the fluctuating component. To address this challenge, the DC coupled radar employs two adaptive tuning architectures: RF coarse-tuning and baseband fine-tuning (Gu and Li 2012). RF coarse-tuning is implemented with an attenuator and a phase shifter at the RF front end of the radar. This tuning phase adds a portion of the transmitted signal to the received signal to eliminate most DC offset. However, due to circuit imperfections, the limited resolutions of the attenuator and phase shifter, the feedback path at the RF front end cannot remove all the DC offsets completely.

To further reduce the residual DC offset, a baseband fine-tuning architecture is adopted. This tuning phase adjusts the amplifier bias to the desired level to allow both high gain amplification and maximum dynamic range at the baseband stage. A block diagram of the fine-tuning process is shown in Fig. 3. In contrast to the AC coupled radar sensor, which is biased at a fixed DC point,

the baseband fine-tuning architecture allows the user to manually adjust the biasing level at the baseband amplifier, making it flexible for a range of practical applications. The baseband amplifier's outputs V_{Q_OUT}/V_{L_OUT} are read dynamically by the microcontroller that transmits the digitalized data via the XBee module to the receiver connected to the PC. To illustrate the baseband fine-tuning process, it is assumed the amplifier has infinite open-loop gain. In this case, the DC level of the amplifier output of the Q channel is

$$V_{Q_OUT} = V_{T_Q} + \frac{R2}{R1}(V_Q^+ - V_Q^-) \quad (3)$$

In Eq. (3) V_{T_Q} is the tuning voltage from the voltage regulator on the RF board, V_Q^+ and V_Q^- are the DC offsets of the I/Q channels, and $R2/R1$ is the closed-loop gain. Depending on the DC value of V_{Q_OUT} , the user manually configures the power supply through a wireless tuning loop to vary the biasing voltage V_{T_Q}/V_{T_I} based on the output until the amplifier output reaches the desired DC level. The same process is applied for I channel. LabView software on the PC is used to complete this tuning loop. With the help of the two DC tuning architectures, the radar sensor can retain low frequency information while removing most of the DC offset.

2.4 Radar signal processing

To convert the acquired baseband signals to a displacement time history, careful signal processing of baseband signals must be conducted. The signal-to-noise ratio (SNR) of the baseband signals is the most critical factor related to displacement measurement accuracy during processing of the raw baseband signals. To increase the SNR, first a low pass filter is applied to the raw baseband signals to minimize high frequency noise. Then DC offset calibration is conducted to obtain accurate final displacement results. Calibrating DC offset values starts by plotting the original baseband signals together to create a trajectory in a constellation diagram.

The trajectory should follow a circular arc, and upon successful DC offset calibration, the arc will lie on the unit circle. One phenomenon that was observed in some of the experimental data was a "bowtie phenomena" when baseband signals are plotted in the constellation graph. Instead of creating a perfect arc, the constellation plot exhibits looping, or a bowtie, as shown in Fig. 4(a). This phenomenon makes DC offset calibration challenging, resulting in erroneous displacement estimates. The source of this phenomenon was found to be a phase delay, or time synchronization error, between baseband I and Q signals. To eliminate this error and ensure that baseband signals are synchronized with one another, they are resampled and aligned. The data before and after the bowtie correction are shown in Fig. 4.

After cancelling the baseband signal phase delay, the DC offset and amplitude values of baseband signals are adjusted automatically until the plotted I/Q trajectory fits the unit circle with the center at the origin. The raw baseband data is corrected by subtracting the DC offset values and then scaling them by the amplitude values. To conduct the DC offset calibration step accurately and efficiently, several methods have been developed to complete this step automatically, including the least square method, the Levenberg-Marquardt method (Zakrzewski *et al.* 2012), compressed sensing method (Xu *et al.* 2012), and the linear demodulation method (Massagram *et al.* 2009). Since each method has different performance under different measurement conditions, a comprehensive strategy to select the appropriate method for corresponding measurement conditions has been established (Guan *et al.* 2014).

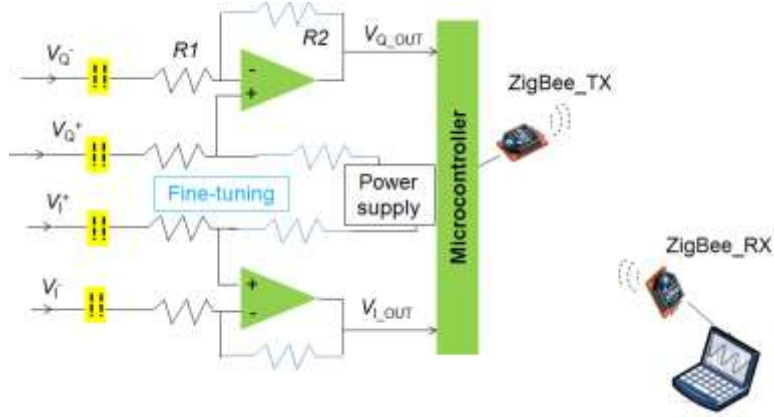
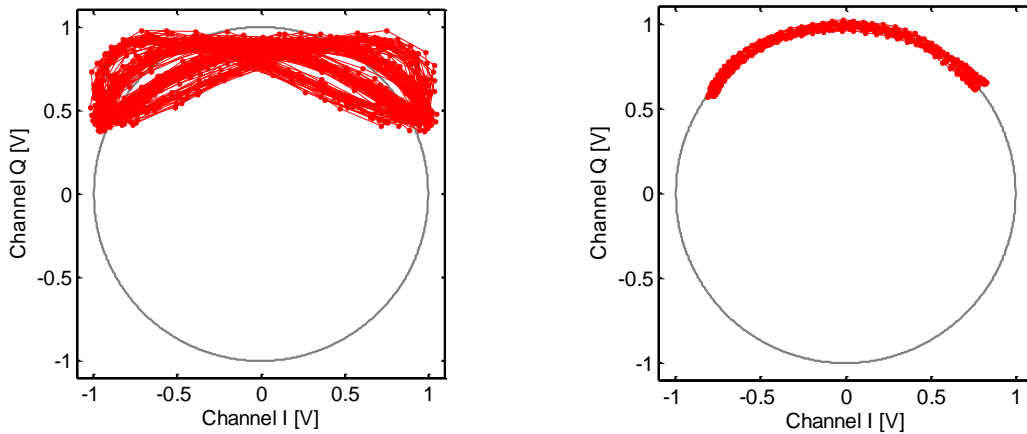


Fig. 3 Block diagram of DC fine-tuning components



(a) Trajectory with baseband synchronization error (b) Trajectory after baseband signal phase delay correction resulting in a “bowtie” effect

Fig. 4 Fitted constellation graph trajectory w/o synchronization error between the baseband signals

After calibrating the DC offsets of the baseband signals, the phase information is determined through arctangent demodulation by

$$\psi(t) = \arctan \left[\frac{B_{Q,corr}(t)}{B_{I,corr}(t)} \right] = \theta + 4\pi x(t)/\lambda + \Delta\varphi \tag{4}$$

$$\varphi(t) = 4\pi x(t)/\lambda \tag{5}$$

where $\varphi(t)$ is proportional to the relative displacement between the subject and the radar. The relative displacement can be obtained as $x(t) = x_0 + \varphi(t)\lambda/4\pi$, where x_0 is the initial distance to the target.

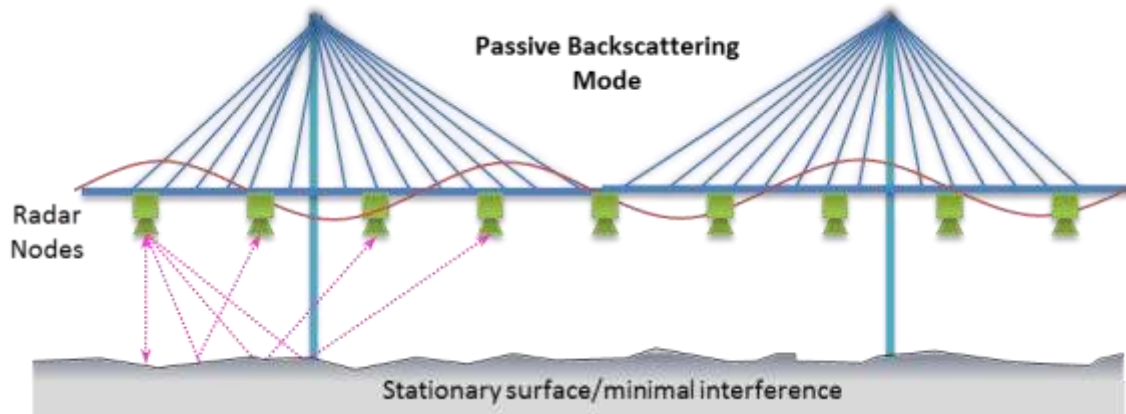


Fig. 5 Passive back scattering mode for bridge application

2.5 Backscattering mode

To employ the radar for practical structural displacement measurement applications, the CW radar may be mounted to the bottom of the bridge deck or the outside surface of the building. In the passive backscattering mode of operation, the ground surface under the bridge or other stationary reference, with adequate reflectivity to radar's signal, serves as the target and reflects signals transmitted by the radar. The radar moves with the vibrating structure and radar's signals modulate the displacement information. An illustration of the backscattering mode for a bridge monitoring application is shown in Fig. 5. Long span bridges may have natural frequencies less than 5 Hz while shorter spans may have frequencies of interest up to 20 Hz. The DC coupled radar has the ability to measure static displacement and natural frequencies up to 20 Hz. The radar has been verified to accurately measure all natural frequencies (from 1.526 Hz to 16.72 Hz) of a seven story building model (Guan *et al.* 2013). One approach to increase the frequency range of measurements is that the radar may be integrated with accelerometers that provide high frequency measurements.

3. Performance characterization

As previously discussed, a high SNR of the baseband signals is critical to obtain accurate displacement measurements. There are several factors that affect the SNR, including the motion amplitude, the distance between the radar and the target, and the target surface material. A series of laboratory experiments have been conducted to characterize radar's accuracy related to these factors. For each trial, one factor was changed while the others were kept constant. The radar's sampling rate can be adjusted easily. Since this paper focuses on the new low frequency (less than 2 Hz) measurement capability of the DC coupled radar, the sampling rate was set at 20 Hz for all tests. The following sections describe these tests for both dynamic displacement and static deflection.

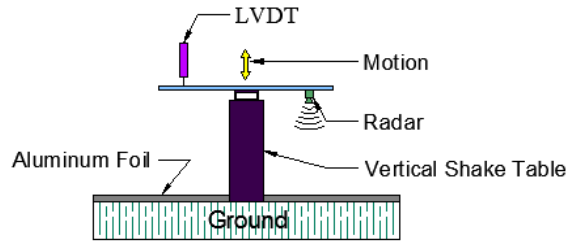


Fig. 6 Dynamic displacement experimental setup

3.1 Laboratory dynamic displacement experiments

A vertical shaker was utilized to generate low frequency sinusoidal motion. A rigid aluminum beam was clamped to the top of the shaker and the DC coupled radar was attached to the other end of the beam to measure the shaker's motion. The antennae of the radar were pointed toward the ground, which acted as the stationary target, at a distance of 50 cm. An LVDT was attached to the beam to provide a reference measurement of the shaker's motion. The motion generated by the shaker, and measurements of LVDT and radar were controlled by a single LabView application running on the PC. The experimental setup is shown in Fig. 6. A series of motions were generated by a shaker with different measurement conditions. A 1.25-Hz sinusoidal motion was generated by the shaker and the amplitude was varied from 1 mm to 10 mm with 1-mm increment, while aluminum foil acted as the target surface. Both the DC coupled and AC coupled radar are capable of measurements up to 20 Hz; the primary difference between the two radars is in the detection of frequencies below 2 Hz. To demonstrate the advantages of DC radar over AC radar in this frequency range, the frequency of the motions in the second set of tests was varied from 0.25 Hz to 2 Hz with 0.25-Hz increments while the amplitude was kept constant at 6.5 mm.

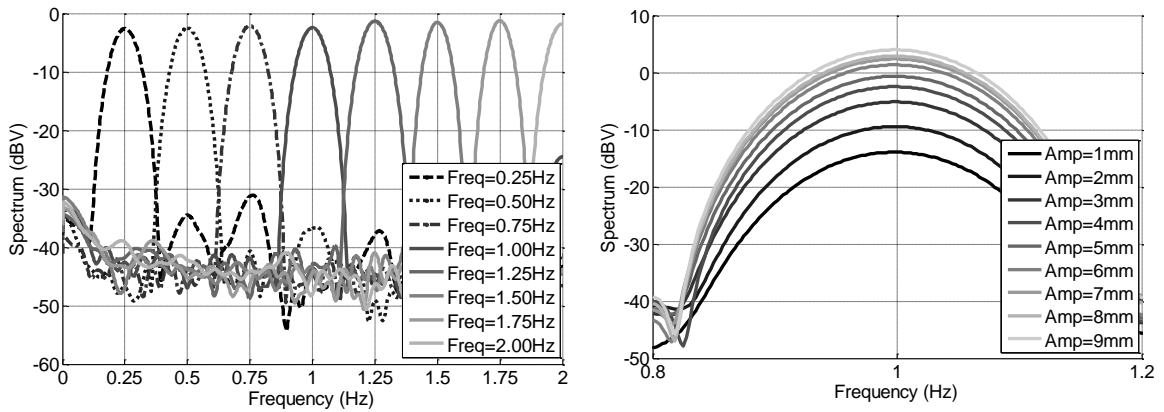
In these series of experiments, the characteristics of baseband signal were investigated first. The baseband signals are a function of target's motion frequency, amplitude, and the distance between the radar and the target. The characteristics of the baseband signals directly affect the radar's displacement measurement accuracy. Power spectral density (PSD) plots of the baseband signals measured at each amplitude and frequency are shown in Fig. 7. Since both baseband signals have similar patterns, only one baseband signal's PSD is shown. Fig. 7(a) shows that the signal power is not related to the frequency of motion being measured, while Fig. 7(b) demonstrates that the baseband signal's power increases as the motion amplitude increases.

The displacement measurement accuracy of radar related to the motion amplitude and frequency was also characterized. For all tests, the motions of the shaker were measured simultaneously by the radar and LVDT. Results from both the radar and LVDT measuring a representative data set of 1.25 Hz sinusoidal motion is shown in Fig. 8. For each measurement condition, three trials were conducted and measurements from the radar and LVDT are compared in the time domain. From the time history record in Fig. 8, the frequency of the radar matches well with the LVDT while some differences in the measured amplitude are observed. To compare the amplitude difference in the time domain, the mean and standard deviation of measurement errors between the radar and the LVDT are calculated and shown in Figs. 9(a) and 9(b). From Fig. 9(a), the mean and standard deviation errors of radar's measurements decrease while the motion amplitude increases because the higher amplitude results in higher a SNR value. In Fig. 9(b) it is

observed that the mean measurement errors are less than 1 mm for all motion frequencies and there is no trend in measurement error related to the motion frequency.

To study the radar’s accuracy related to its distance from the target, the radar was attached to a horizontal shaker to measure motion of the shaker. A constant 1-Hz sinusoidal motion with a 10-mm amplitude was generated by the horizontal shaker. A 2 m × 1.5 m metallic board served as a reflection surface. The distance between the radar’s antenna and the target surface was varied from 1 m to 7 m in 1-m increments. The experimental setup is shown in Fig. 10(a).

The PSDs of baseband signals related to different distances are shown in Fig 10(b). From the spectrum plot of baseband signals related to different distances in Fig. 10(b), the signal’s power tends to decrease with increased distance. This trend is as expected since the signal power of baseband signals decreases as the target distance increases. For the distance of 3 m, the signal’s power is the smallest due to the signal’s power reduced by the signals reflected from the ground surface.



(a) PSD of baseband signals vs. different frequencies (b) PSD of baseband signals vs. different distances

Fig. 7 PSD of baseband signals related to different factors

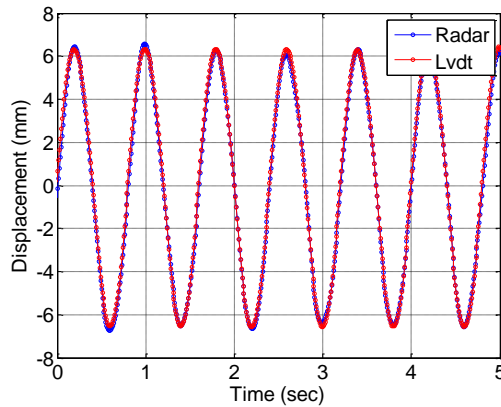
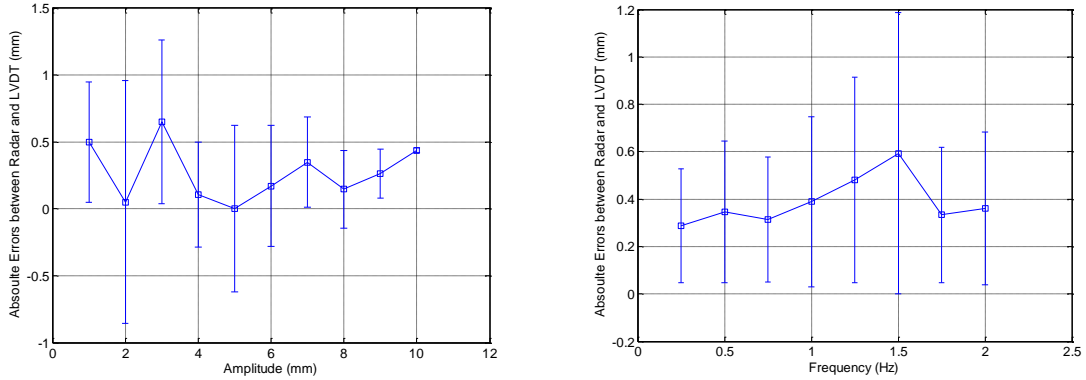


Fig. 8 A representative measurement results of 1.25 Hz sinusoidal motion by radar and LVDT

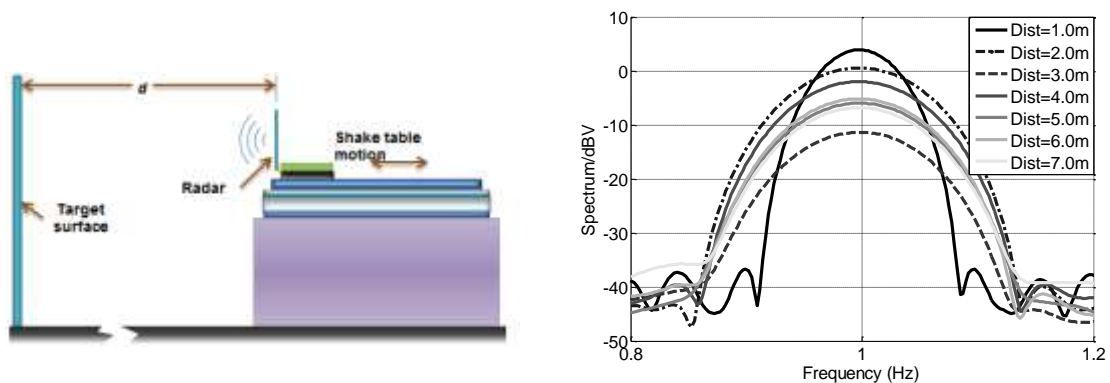


(a) Absolute errors between radar and LVDT vs. different motion amplitudes with one standard deviation indicated. (b) Absolute errors between radar and LVDT vs. different motion frequencies with one standard deviation indicated.

Fig. 9 Measurement errors between radar and LVDT vs. different amplitudes and frequencies

To quantify the radar’s errors, an LVDT measured the shaker’s motion simultaneously. Results from both the radar and LVDT measuring a representative data set of 1.0 Hz sinusoidal motion with 1 m distance between the radar and target are shown in Fig. 11. The mean and standard deviation errors of the motion amplitude between the radar and the LVDT are shown in Fig. 12.

From Fig. 12 the measurement from the radar has a sub-millimeter level accuracy when the distance is less than 6 m. As the distance increases, both the mean and standard deviation of absolute errors increase due to attenuated signal power and increased signal noise, demonstrating that the radar has less measurement accuracy and consistency at larger target distances. For practical SHM applications, if the distance between the radar and target is less than 6 m, sub-millimeter accuracy may be achieved. Approaches for increasing the radar’s measurement distances are discussed in the conclusions.



(a) Experimental setup of radar’s measurement performance vs. target distance (b) Spectrum of radar’s baseband signals vs different target distances

Fig. 10 Dynamic displacement experimental setup and measurement results

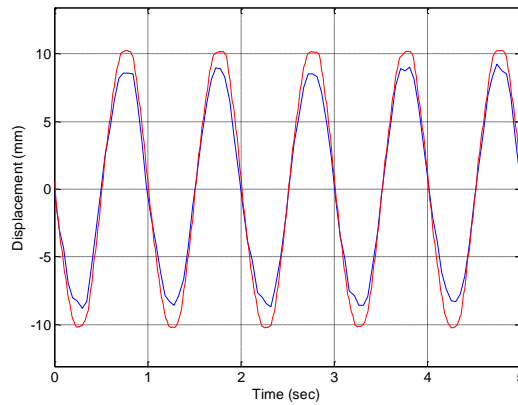


Fig. 11 A representative measurement results of 1.0 Hz sinusoidal motion by radar and LVDT with 1 m distance between the radar and target

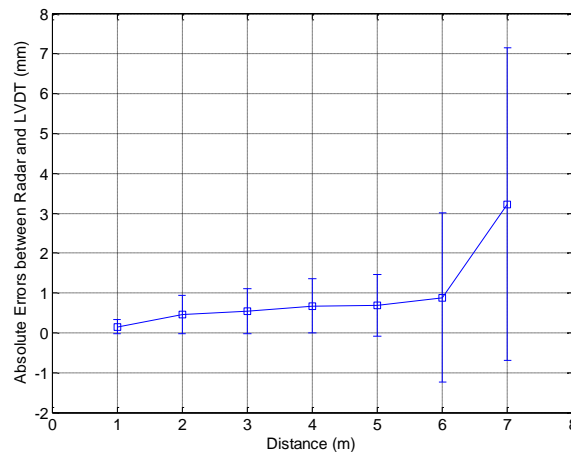


Fig. 12 Absolute errors between radar and LVDT vs. target distance, with one standard deviation indicated

3.2 Laboratory static deflection measurement experiments

Another promising application of the DC coupled radar is the measurement of static structural deflection. To demonstrate and characterize the radar’s static deflection measurement performance, an aluminum beam with dimensions of 180 cm × 30 cm × 0.6 cm and variable vertical clearance was used as a test bed. Different sets of load combinations were applied to the beam to create a range of mid-span deflections. The experimental setup is shown in Fig. 13(a). The beam height (and thus the target distance) was held constant at 1.25 m and aluminum foil was used to reflect the signals. The deflection was kept at about 10 mm and aluminum foil served as the reflection surface. The radar’s antennae were attached to the bottom side of the mid-span of the beam. An LVDT was attached to the beam to measure the mid-span deflections simultaneously.

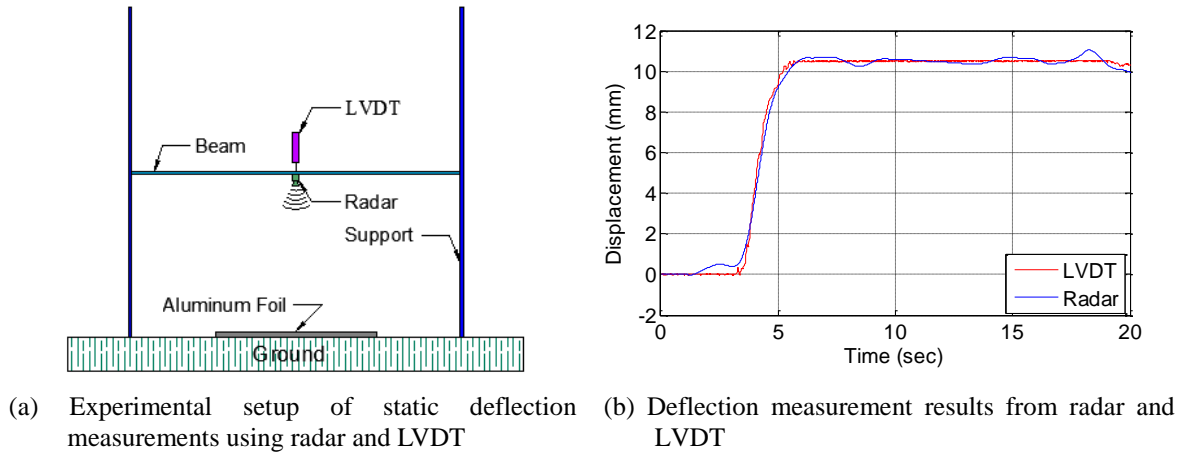


Fig. 13 Static deflection experimental setup and measurement results

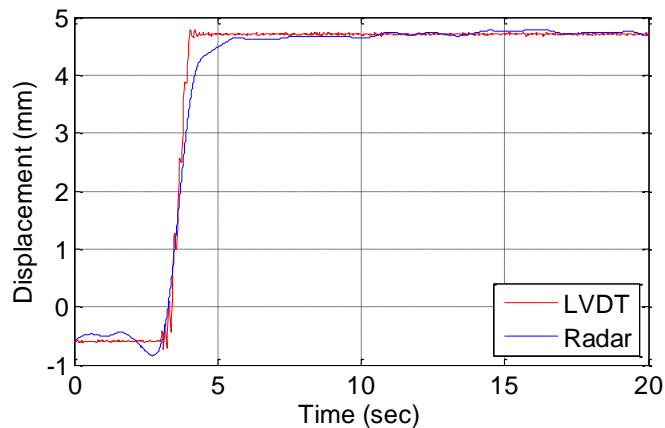


Fig. 14 Measurement results of radar and LVDT

To reduce the signal noise to achieve constant displacement measurements before and after the application of the load, a moving average function was applied to the displacement signal. This approach is only appropriate for static measurements since it suppresses any dynamic component of the signal. The rate at which the displacement varies during a test will determine the number of data points that should be used for the moving average calculation; the data presented in this paper utilized a 100-point moving average.

One of the experimental results is shown in Fig. 13(b). From the time history record, the radar captures the entire process of the static deflection experiment, with a large jump in displacement observed when the load is placed on the beam. The difference in the total deflection changes between the radar and LVDT is less than 1 mm. In Fig. 13(b) some fluctuations in the radar measurement are observed relative to the constant measurement of the LVDT. From Fig. 11, it should be noted that similar signal errors ($< 1\text{mm}$) were observed in the dynamic displacement

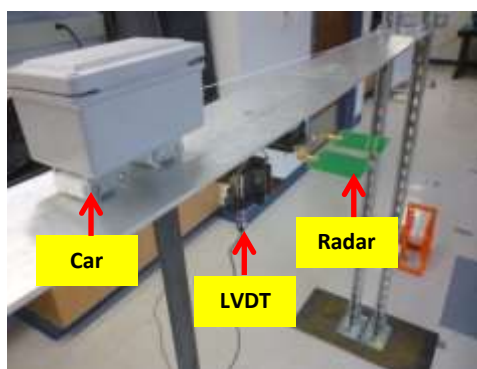
tests conducted at similar target distance. In the static deflection test results the fluctuations are more observable due to the flat reference signal.

3.3 Field static deflection measurement experiments

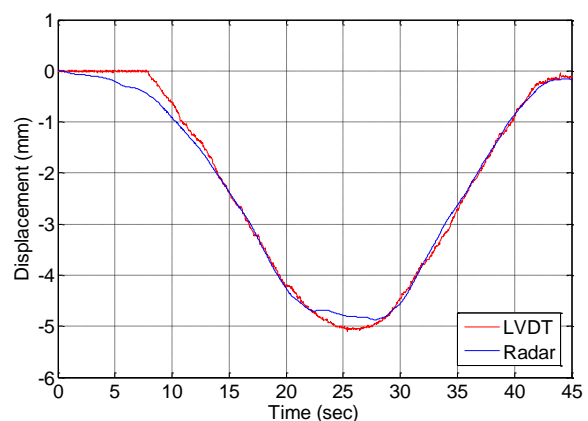
To evaluate the static deflection measurement performance in the field, where higher measurement noise levels are expected, the static deflection experimental setup was moved outside. The beam height was still held constant at 1.25 m and aluminum foil was used to reflect the signals. Results from both the radar and LVDT measuring a representative data set with about 5mm deflection amplitude are shown in Fig. 14. From Fig. 14, the accuracy of the measurements from the field tests exhibit similar trends as the laboratory experiments.

3.4 Laboratory moving load experiments

To simulate the process of measuring deflections of a moving vehicle traveling across a bridge, a moving load laboratory experiment was conducted. The aluminum beam height was set at 1.25 m. A small moving car was used to create deflections of the aluminum beam. A light rope in tension was used to guide the loaded car along the bridge at a slow speed. The total weight of the car is about 0.7 kg. One DC coupled radar was attached to the mid-span of the beam with the antennae pointing toward the floor below and an LVDT provided the reference measurement. The car moved from one end of the beam to the other while the sensors simultaneously measured the mid-span deflection of the beam. The experimental setup is shown in Fig. 15(a). The measurements of both the radar and the LVDT at mid-span are shown in Fig. 15(b). From Fig. 15(b), the radar captures the whole process of the car moving across the bridge, the shape of the deflection measured by radar and LVDT are similar while the maximum difference of the amplitude is about 0.3 mm.



(a) Experimental setup of moving load tests using radar and LVDT



(b) Measurement results from both radar and LVDT

Fig. 15 Experimental setup of moving load tests and absolute errors between radar and LVDT

4. Conclusions

In summary, the DC coupled radar demonstrates reasonable accuracy when measuring dynamic displacements in a laboratory environment. In addition, the DC coupled radar demonstrates the potential to capture static deflections accurately in both the laboratory and outdoor environments. The moving load experiment further demonstrates the static and low frequency measurement capabilities of the DC coupled radar. The accuracy of the radar measurements is sub-millimeter when the measurement distance is less than 6 m.

Ongoing research is underway to address remaining challenges limiting the practical application of the radar. This research includes integrating the radar sensor with other sensors (such as accelerometers) to expand its application for a wide range of SHM studies. In addition, increasing the measurement range of the current radar is being investigated through modifications to the target. The focus of this investigation is on increasing the SNR of the baseband signals to increase the radar's measurement range. A surface with good reflectivity can increase the SNR of the signal by decreasing signal attenuation (Guan *et al.* 2014). Another approach that has been verified to increase baseband signal SNR is the use of a transponder at the target point to amplify the signal before it is sent back to the radar's receiver (Gu *et al.* 2012). Changing the hardware design of the radar also offers opportunities for improved performance at larger measurement distances. Specifically, increasing the carrier frequency of the radar improves the signal power by decreasing the beamwidth of the signal. A 24 GHz radar system is currently under investigation to address the limitations of the current hardware. In the future, the DC coupled radar performance will be verified on a full-scale structure and the signal processing will be embedded on the microprocessor of the wireless unit.

Acknowledgments

The authors gratefully acknowledge the support of this research by the National Science Foundation under grant CMMI 1131506 (Dr. George A. Hazelrigg, Program Director). Sensor performance tests were assisted by Juliana Rochester and Mackenzie Matthews.

References

- Chan, T.H., Ashebo, D.B., Tam, H., Yu, Y., Chan, T., Lee, P. and Gracia, E.P. (2009), "Vertical displacement measurements for bridges using optical fiber sensors and CCD cameras – a preliminary study", *Struct. Health Monit.*, **8**(3), 243-249.
- Gu, C. and Li, C. (2012), "DC coupled CW radar sensor using fine-tuning adaptive feedback loop", *Electron. Lett.*, **48**(6), 334-345.
- Gu, C., Wang, G., Rice, J.A. and Li, C. (2012), "Interferometric radar sensor with active transponders for signal boosting and clutter rejection in structural health monitoring", *Proceedings of the IEEE MTT-S International Microwave Symposium, Montreal, Canada, June 2012*.
- Gu, C., Li, C., Lin, J., Huangfu, J. and Ran, L. (2010), "Instrument-based noncontact doppler radar vital sign detection system using heterodyne digital quadrature demodulation architecture", *IEEE T Instrum. Meas.*, **59**(6), 1580-1588.
- Gu, C., Li, R., Jiang, S.B. and Li, C. (2011), "A multi-radar wireless system for respiratory gating and accurate tumor tracking in lung cancer radiotherapy", *Engineering in Medicine and Biology Society*,

- Proceedings of the 2011 Annual International Conference of the IEEE.*
- Guan, S., Rice, J.A., Li, C. and Gu, C. (2014), "Automated DC offset calibration strategy for structural health monitoring based on portable CW radar sensor", *IEEE T Instrum. Meas.*, in press.
- Guan, S., Rice, J.A., Li, C. and Wang, G. (2014). "Bridge deflection monitoring using small, low-cost radar sensors", *Proceedings of the Structures Congress 2014*, Boston, MA.
- Guan, S., Rice, J.A., Rochester, J., Wang, G. and Li, C. (2013), "Performance comparison of DC and AC coupled radars for structural health monitoring", ANCRiSST, Ulsan, Korea.
- Lee, J.J. and Shinozuka, M. (2006), "A vision-based system for remote sensing of bridge displacement", *NDT & E Int.*, **39**(5), 425-431.
- Massagram, W., Lubecke, V.M., Host-Madsen, A. and Boric-Lubecke, O. (2009), "Assessment of heart rate variability and respiratory sinus arrhythmia via Doppler radar", *IEEE T Microwave Theory Tech.*, **57**(10), 2542-2549.
- Moschas, F. and Stiros, S. (2014), "Three dimensional dynamic deflections and natural frequencies of a stiff footbridge, based on measurements of collocated sensors", *Struct. Control Health Monit.*, **21**(1), 23-42.
- Rice, J.A, Gu, C., Li, C. and Guan, S. (2012), "A radar-based sensor network for bridge displacements", *SPIE*, San Diego, 3.
- Rice, J.A., Mechitov, K., Sim, S.H., Nagayama, T., Jang, S., Kim, R., Spencer Jr., B.F., Agha, G. and Fujino, Y. (2010). "Flexible smart sensor framework for autonomous structural health monitoring," *Smart Struct. Syst.*, **6**(5-6), 423-438.
- Rossi, G., Marsili, R., Gusella, V. and Gioffre, M. (2002), "Comparison between accelerometer and laser vibrometer to measure traffic excited vibrations on bridges", *Shock Vib.*, **9**(1), 11-18.
- Stiros, S.C. (2008), "Errors in velocities and displacements deduced from accelerographs: An approach based on the theory of error propagation", *Soil Dyn. Earthq. Eng.*, **28**(5), 415-420.
- Stiros, S. and Psimoulis, P. (2012), "Response of a historical short-span railway bridge to passing trains: 3-D deflections and dominant frequencies derived from Robotic Total Station (RTS) measurements", *Eng. Struct.*, **45**, 362-371.
- Xu, W., Gu, C., Li, C. and Sarrafzadeh, M. (2012), "Robust Doppler radar demodulation via compressed sensing", *Electron. Lett.*, **48**(22), 1428-1430.
- Yang, J., Li, J.B. and Lin, G. (2006), "A simple approach to integration of acceleration data for dynamic soil-structure interaction analysis", *Soil Dyn. Earthq. Eng.*, **26**(8), 725-734.
- Zakrzewski, M., Raitinen, H. and Vanhala, J. (2012), "Comparison of center estimation algorithms for heart and respiration monitoring with microwave doppler radar", *IEEE Sens. J.*, **12**(3), 627-634.